

Spectral response of scintillating fibres

Z. Papandreou*, B.D. Leverington and G.J. Lolos

Department of Physics, University of Regina, Regina, SK, S4S 0A2, Canada

Abstract

The spectral response of PHT-0044 (blue) and BCF-20 (green) scintillating fibres was measured as a function of wavelength using a UV LED. It was observed that significant spectral strength from the PHT-044 fibres was missing compared to manufacturer's specifications at the origin of the source, shifting the peak value of the spectrum to significantly higher values in wavelength. In contrast, the corresponding shift for the BCF-20 fibres was minimal. The mechanisms responsible for the observed behavior are discussed herein. Moreover, the attenuation length for each fibre type was extracted and studied as a function of wavelength. Finally, the measured fibre spectra were convolved with the wavelength response from a typical bi-alkali photo multiplier as well as a green-sensitive silicon photo multiplier, yielding the number of photoelectrons, which is shown to be consistent with the numbers extracted from cosmic-ray and photon-beam data.

Key words: scintillating fibres, wavelength response, optical transmission, electromagnetic calorimeter

PACS: 29.40.Mc, 29.40.Vj

1 Introduction

2 The study in this paper was undertaken in the context of determining the opti-
3 mal type of scintillating fibres to be coupled to the electronic front-end readout
4 of the electro-magnetic barrel calorimeter (BCAL) for the GlueX project. This
5 experiment aims to elucidate *confinement* in Quantum Chromodynamics, by
6 searching for hybrid mesons that possess gluonic degrees of freedom and ex-
7 otic quantum numbers, and arise from photoproduction at 9 GeV [1,2]. To
8 achieve this goal, amplitude analyses on numerous exclusive reactions must
9 be carried out to determine the J^{PC} quantum numbers of produced exotic

* Corresponding author. Tel.: +1 306 585 5379; fax: +1 306 585 5659
Email address: zisis@uregina.ca (Z. Papandreou).

10 mesons, which decay into photons and charged particles. Clearly, an overall
11 hermetic detector with adequate resolution is essential, and the BCAL is a
12 crucial subsystem. Indeed, this calorimeter will cover 11° to 126° with respect
13 to the beam direction, and will be charged primarily with the detection of
14 photons resulting from $\pi^0 \rightarrow \gamma\gamma$ and $\eta \rightarrow \gamma\gamma$ decays in the 40 MeV to 4 GeV
15 energy range.

16 Significant contribution to the energy and timing resolution as well as detec-
17 tion threshold arises from the resulting photo-statistics associated with the
18 traversal of neutral or charged particles through the BCAL. At the end of the
19 readout this feature is quantified by the number of produced photoelectrons.
20 Therefore, it is important to optimize the production, transport and collection
21 of optical photons and their conversion to photoelectrons for a given energy
22 deposition in the calorimeter, while accounting for attenuation.

23 The BCAL will be comprised of a lead and scintillating fibre matrix, consisting
24 of ~ 200 layers of lead sheets, each of 0.5 mm thickness, and 1-mm-diameter,
25 multi-clad, scintillating fibres (SciFi), bonded in place using BC-600 optical
26 epoxy¹. The detector will consist of 48 modules each 390 cm long and with
27 a trapezoidal cross section, and will form a cylindrical shell with inner and
28 outer radii of 65 cm and 90 cm, respectively. The simulated sampling fraction
29 – fraction of photon energy deposited in the SciFi’s with respect to the total
30 energy deposited in the module – is 12.5%. Two full-sized prototype modules
31 were constructed: Module 1 was built entirely of PHT-0044² fibres, whereas
32 Module 2 was built with a combination of PHT-0044 and BCF-20 fibres.

33 The BCAL will be deployed inside the GlueX detector’s super-conducting
34 solenoid. The central field of the solenoid is 2.2 T, resulting in substantial
35 magnetic field strength and gradients near the BCAL ends, so using vacuum
36 PMT’s with short light guides is not possible. The leading option is to use
37 silicon photomultipliers (SiPM) coupled to compact light guides. These devices
38 are immune to large magnetic fields and typically have their peak quantum
39 (QE) and photon-detection (PDE) efficiencies in the green optical region. Our
40 collaboration has been working with SensL³ to develop large-area SiPM arrays
41 (SiPMPlus), in order to match the GlueX readout cell size.

42 The breakdown of this paper is as follows. The scintillation mechanism is
43 briefly recounted in Section 2, the experimental measurements are described
44 in Section 3, the data analysis is presented in Section 4 and the conclusions
45 in Section 5.

¹ St. Gobain Crystals & Detectors, Newbury, OH, USA (www.bicron.com)

² PolHiTech SRL, 67061 Carsoli (AQ), Italy (www.polhitech.it)

³ SensL, Blackrock, Cork, Ireland (www.sensl.com)

46 **2 Scintillation mechanism**

47 The chemical and optical properties of scintillating materials have been pre-
 48 sented elsewhere [3–5] and are recounted briefly herein. Such materials are
 49 composed of a chemical base, usually polystyrene or polyvinyltoluene, and
 50 one or more dyes that are added to improve the quantum yield of the scintil-
 51 lator and to wavelshift the scintillation light to longer wavelengths.

52 The fluorescence mechanism responsible for scintillation light occurs in the
 53 base materials and the additive dyes. It relies on the atomic structure of car-
 54 bon atoms, where electron excitation is followed typically via a two-step mech-
 55 anism, the first involving a non-radiative and the second a radiative decay. It
 56 is the latter step that produces fluorescence, or scintillation light [3].

57 The scintillation material itself suffers from light absorption and a quantum
 58 yield of a few percent only. Primary dyes have a quantum yield typically
 59 over 80% and their optimum concentration in the mixture is about 1% by
 60 weight [3,4] but are also subject to self-absorption. A secondary dye, in a much
 61 lower concentration (around 0.01%), resolves this issue by quickly absorbing
 62 the primary emission and wavelshifting it to a longer wavelength. This process
 63 “extends” the primary attenuation length from a few cm up to several meters,
 64 and indeed SciFi’s emit in the blue or green region and have attenuation
 65 lengths over 3.5 m. Moreover, the concentrations of the dyes can be tuned to
 66 achieve either higher light yield at the expense of attenuation length or the
 67 reverse.

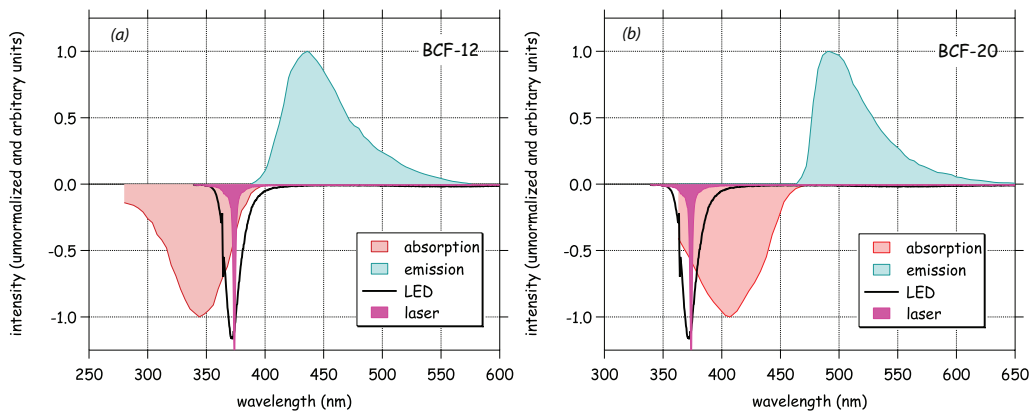


Fig. 1. Emission and absorption spectra from the secondary dye of (a) BCF-12 and (b) BCF-20 fibres. Also shown are the stimulated wavelength ranges from the 373 nm LED and 375 nm laser used in our measurements, as discussed below. All curves have been arbitrarily normalized to facilitate the comparison of their spectral shapes. (colour online)

68 The attenuation length depends on the self-absorption of the materials and
 69 reflection losses as the photons travel down the fibre [6]. This is illustrated in

70 manufacturer’s absorption and emission spectra for the second dye in BCF-12
71 and BCF-20 as shown in Fig. 1, together with the stimulated wavelengths
72 from the two light sources used in our experiment. The overlap between the
73 absorption and emission spectra in Fig. 1 is minimal, thus resulting in long
74 attenuation length for these fibres. The integral of the transmitted light in-
75 tensity decreases linearly as a function of the distance that the light travels in
76 the fibre, i.e. there is an exponential loss of photons. The various wavelength
77 regions exhibit differing slopes in these curves, with the shorter wavelengths
78 following steeper slopes [3].

79 In this paper, our investigation focused on the measurement of wavelength
80 spectra from 1-mm-diameter PHT-0044 and BCF-20 SciFi and the subse-
81 quent analysis to extract the short- and long-attenuation lengths as well as
82 the dependence of the attenuation length on wavelength. Both SciFi types
83 are composed of a core of polystyrene and two layers of polymethylmethacry-
84 late cladding: the first from acrylic and the second from fluor-acrylic material,
85 having thicknesses of 3% and 1% of the fibre’s diameter⁴. An important issue
86 in the data analysis is the normalization of the light produced at the source,
87 corresponding to near-zero fibre length. To this end, manufacturers’ source
88 spectra were examined and compared to our nearest measurements (1 mm
89 fibre length). The properties of PHT-0044 and BCF-12 are quite similar, in
90 terms of peak emission and attenuation length. Source spectra are not avail-
91 able for the former, and this is why the BCF-12 spectra were used, instead.

92 **3 Measurements**

93 For the measurements reported herein, a LED light source, a spectro-photometer
94 and the tested SciFi were coupled together in a robust and reproducible man-
95 ner. The SD2000 dual-channel fibre optic spectro-photometer⁵ is based on a
96 blazed diffraction grating with a 50 μm wide slit and features a high-sensitivity
97 2048-element linear CCD array that provides high response and excellent op-
98 tical resolution from 200-1100 nm. This device had been calibrated by the
99 manufacturer, and the provided specifications indicated a wavelength differ-
100 ence, $|\delta\lambda|$, between expected and measured values, never exceeding 0.3 nm for
101 any given pixel on the CCD. The SD2000 employs an external ADC1000-USB
102 A/D converter to communicate with a PC running commercial software. The
103 spectro-photometer had an integration window of 150 μs and measured the
104 wavelength region of 340-1020 nm in over 2000 bins, resulting in a resolution
105 of ~ 3.3 bins/nm (or 0.3 nm). As a result, although the spectral shapes appear
106 jagged at each wavelength, upon close inspection the overall behavior of the

⁴ St. Gobain Crystals & Detectors, Scintillating Optical fibres Brochure 605.

⁵ Ocean Optics Inc., Dunedin, FL, USA (www.oceanoptics.com)

107 data was stable, as evidenced by their long-wavelength tails that overlapped
108 above 500 nm as expected, since at those wavelengths there is little absorption
109 of light. This feature will be demonstrated below. Sample dark spectra were
110 obtained and these had negligible effect on the measured spectra with UV
111 light.

112 For our measurements, a RLU370-1.7-30 ultra violet LED⁶ was employed,
113 with a peak emission wavelength of 373 nm, a spectrum bandwidth of 13 nm,
114 and typical radiant flux of 1.7 mW. Selected measurements were also per-
115 formed using a 375 nm PicoQuant PDL 800-B picosecond pulsed diode laser
116 with LDH-P-C-375B laser head⁷. A comparison of the spectra from the LED
117 and the laser, as measured directly with the spectro-photometer, are shown in
118 Fig. 2. These demonstrate that: a) the spectro-photometer had been correctly
119 calibrated versus wavelength by its manufacturer, since the peak emission of
120 the LED and the laser indeed were measured to be at 373 nm and 375 nm,
121 respectively, and the peak widths were 13 ns and 1 ns, in agreement with man-
122 ufacturers' specifications; b) There is no significant contribution from these
123 light sources to the intensity of the measured fibre spectra in the wavelength
124 range of interest, since the broad LED peak at ~ 560 nm is only at the few
125 percent level and does not fall in the excitation region of the fibres. In any
126 case, this peak does not appear in the fibre spectra when the LED is posi-
127 tioned perpendicularly to the tested SciFi. The spectro-photometer was also
128 used to measure the spectra of other LEDs at 470 nm and 590 nm and was
129 found equally accurate.

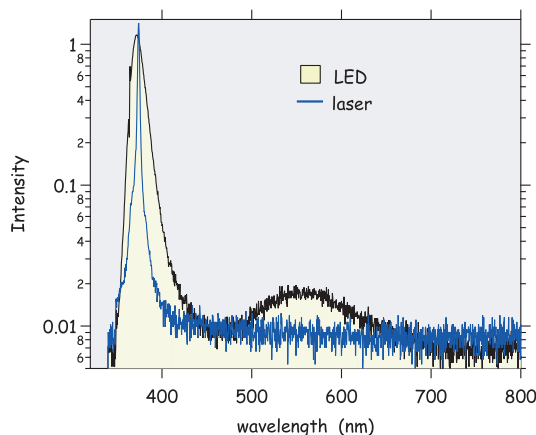


Fig. 2. Comparison of the emission spectra of the LED and the laser as measured directly, using the spectro-photometer, and plotted on a logarithmic scale. Details are provided in the text. (colour online)

130 The fibre under test was clamped in place horizontally until it was taut, with
131 one end held via a clamp on a lab stand while the other was glued through

⁶ Roithner Lasertechnik, Vienna, Austria (www.roithner-laser.com)

⁷ PicoQuant GmbH, Berlin, Germany (www.picoquant.com)

132 a SMA connector using BC-600 epoxy. Once the glue had cured, the fibre
 133 end at the tip of the SMA connector was polished using three progressive
 134 grades of polishing paper (coarse, 12 μm and 3 μm grit) and a polishing puck,
 135 from a Clauss⁸ fibre Optic Polishing kit (PK-2000), and was cleaned using
 136 ethyl alcohol and KimWipes to remove metallic dust originating from the tip
 137 of the SMA connector. Finally, the SMA end was coupled to the spectro-
 138 photometer's slave channel. This method allowed for easy and reproducible
 139 coupling of fibre to spectro-photometer. The setup was made robust to protect
 140 against displacing the test fibre and was leveled to avoid any curvature in
 141 the test fibres, which was shown to affect the intensity of the detected light,
 142 although it does not influence the shape of the spectra.

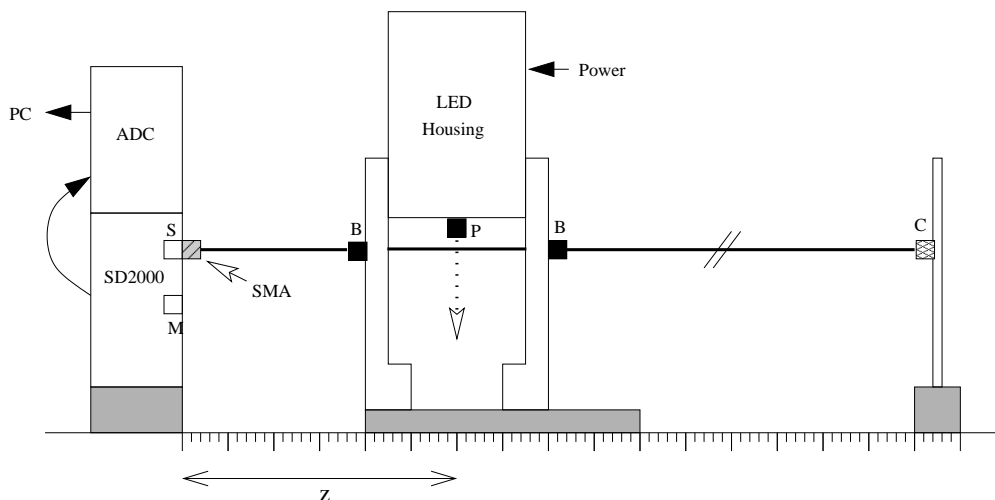


Fig. 3. Schematic drawing of the experiment. The test fibre is shown as the bold horizontal line: on the right it is clamped to a lab stand (C), in the middle it threads through the legs of the LED support stand via barrels (B) having 1 mm inner diameter holes and external threads that mount on the support frame and on the left it is connected to the slave channel (S) of the SD2000 spectro-photometer by an SMA connector. The SD2000 connects to the ADC via a flat-ribbon bus and the ADC, in turn, connects to a PC via a USB cable. The vertical arrow pointing downwards from the LED housing indicates the direction of the incident light through its port (P) onto the test fibre. The horizontal displacement of the light direction to the entrance of the SD2000 master channel is our distance parameter, z . This figure is not to scale: for example, the LED's port is a lot closer to the fibre than implied in this schematic.

143 The LED was installed in a commercial housing and was mounted on a spe-
 144 cially designed stand that could slide on the lab bench and translated across
 145 the length of the fibre (from 8 cm to 380 cm) in a parallel fashion, guided by
 146 a set of aligned, steel ruled guides. A schematic drawing of the setup is shown
 147 in Fig. 3. It should be noted that in that figure the distance of the LED hous-
 148 ing port (P) to each fibre tested was 3 mm and held constant to maintain a

⁸ The PK-2000 can be obtained from a large number of fibre accessories vendors.

149 consistent beam profile. With this setup, relative comparisons of the measured
150 light intensity along the length of a given fibre were possible. However, due to
151 the different level of polish of each fibre, absolute comparisons from one fibre
152 to another were not possible as far as the measured intensity went, although
153 the spectral shapes were unaffected and could still be compared.

154 All measurements were carried out in complete darkness in our lab. However,
155 since the core of blue-emitting scintillating fibres can be damaged by prolonged
156 exposure to UV light, yellow, UV-absorbing film (TA-81-XSR⁹) was used to
157 cover all fluorescent overhead and incandescent desk lights in our detector test
158 laboratory during the preparation and setup stages.

159 4 Results

160 This section is subdivided as follows. The fitting of the wavelength spectra for
161 distances from 8 cm to 380 cm is presented first, since this method was entirely
162 self consistent and independent of assumptions on the manufacturer's source
163 (0 cm) spectra. This is followed in sequence by a different set of measurements
164 from 1 mm to 20 mm and a comparison of those results to manufacturer's spec-
165 tra. Finally, the effect of two different photosensors on the measured spectra
166 is shown and the number of photoelectrons is extracted and compared to lit-
167 erature.

168 4.1 Fitting the emission spectra

169 The measured spectra for the BCF-20 and PHT-0044 fibres are shown in Fig. 4
170 at 8 cm from the source; these are typical of the spectra measured for all other
171 source distances. On one hand, the BCF-20 spectra are well described by a
172 Moyal distribution function plus a flat background:

$$173 \quad f(x, a, \mu, \sigma, b) = a \cdot \exp\left(-\frac{1}{2}\left(\frac{(x - \mu)}{\sigma} + e^{-(x - \mu)/\sigma}\right)\right) + b \quad (1)$$

174 as is evident in Fig. 4a where the fit to Eq. 1 is shown. On the other hand,
175 the PHT-0044 fibre spectra require a sum of two Moyal functions plus a flat
176 background, as shown in Fig. 4b. The results of fits to Moyal functions for
177 spectral measurements at LED distances ranging from 8 to 380 cm for the
178 PHT-0044 and BCF-20 fibres are shown in Fig. 5. The Moyal distribution is
179 often used as a good approximation to the Landau distribution [7].

⁹ Window Film Systems, London, ON, Canada (www.windowfilmsystems.com)

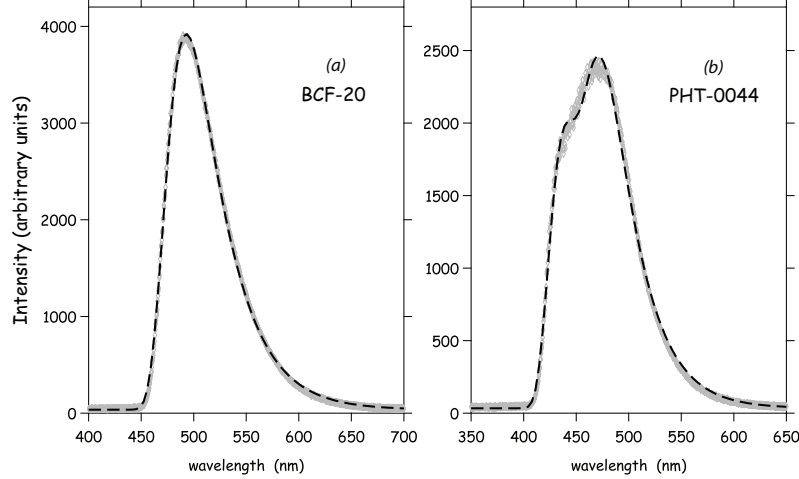


Fig. 4. (a) The emission spectrum for the BCF-20 fibre (grey band) is shown with the source located at 8 cm from the spectro-photometer and the results of a fit (dashed line) to a Moyal function plus a flat background; and (b) The emission spectrum (grey band) for the PHT-0044 fibre with the source located at 8 cm from the spectro-photometer with the results of a fit (dashed line) to a sum of two Moyal functions plus a flat background.

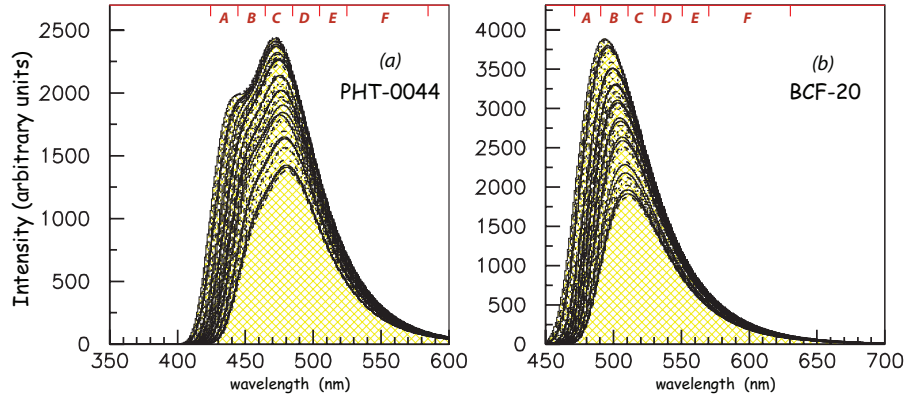


Fig. 5. The results of fits to Moyal functions for spectral measurements at source distances ranging from 8 to 380 cm for (a) PHT-044 and (b) BCF-20 fibres. The wavelength ranges labeled *A* through *F* in the plots will be referenced later in this paper. (colour online)

180 The single Moyal function fits have 4 parameters including an amplitude (a),
 181 a characteristic wavelength and width (given by μ and σ) and the background
 182 term (b). The fits involving a sum of two Moyal functions introduce three
 183 additional parameters. The BCF-20 fibre spectral fits are characterized by a
 184 single wavelength (μ) and width (σ) and the PHT-0044 fits are characterized
 185 by two wavelengths (μ_1 and μ_2) and corresponding widths (σ_1 and σ_2). The
 186 dependence of these fit parameters on LED distance is shown in Fig. 6. The
 187 integral of the background term over wavelength from 400 to 700 nm is about
 188 5% of the integral of the spectra over this same wavelength range.

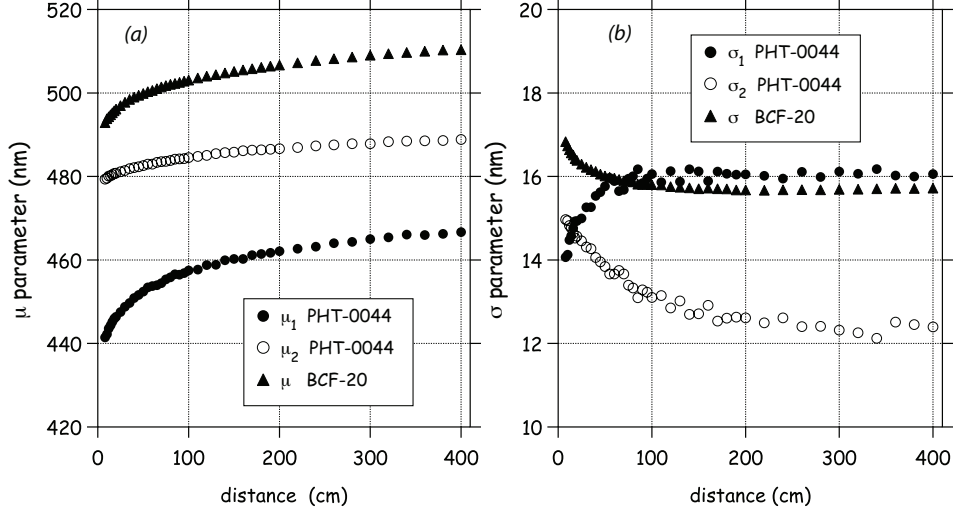


Fig. 6. Dependence of the Moyal fit parameters (a) μ and (b) σ as a function of source distance for the PHT-0044 and BCF-20 fibres.

189 4.2 Attenuation length versus wavelength

190 The Moyal fits described above were integrated over wavelength for the two
 191 fibres for various source distances. Six ranges of wavelength (labeled *A* through
 192 *F*) over which the integrals were performed are indicated in Fig. 5 for the two
 193 fibres. The central (middle of each bin) wavelengths are indicated in the legend
 194 of the plots in Fig. 7. These data were fit to an exponential of the form:

$$195 \quad I(d) = I_0 + \alpha \cdot e^{-(d-d_0)/\lambda} \quad (2)$$

196 For the fits shown, the floor term was set at about 10% of the maximum value
 197 for the data in a particular wavelength range. The d_0 was not a fit parameter
 198 but rather was determined by the starting point of the fit which was $d_0 = 8$ cm
 199 for all the wavelength ranges except for the wavelength range labeled *A*. The
 200 fit parameter λ is the attenuation length and its dependence on wavelength
 201 for the two fibres is shown in the left panel of Fig. 8. Such behaviour was first
 202 reported in reference [3].

203 The attenuation lengths in the right panel of Fig. 8 were obtained by plotting
 204 the value of the Moyal fit function as a function of distance at discrete wave-
 205 lengths and fitting to an exponential. Note the structure in this dependence
 206 around 460 nm to 470 nm that corresponds to the region of the second peak in
 207 Fig. 5. This is a persistent feature and not an artifact of our measurements or
 208 the spectro-photometer response, and shows faintly in the left panel of Fig. 8
 209 due to the lower resolution in that method.

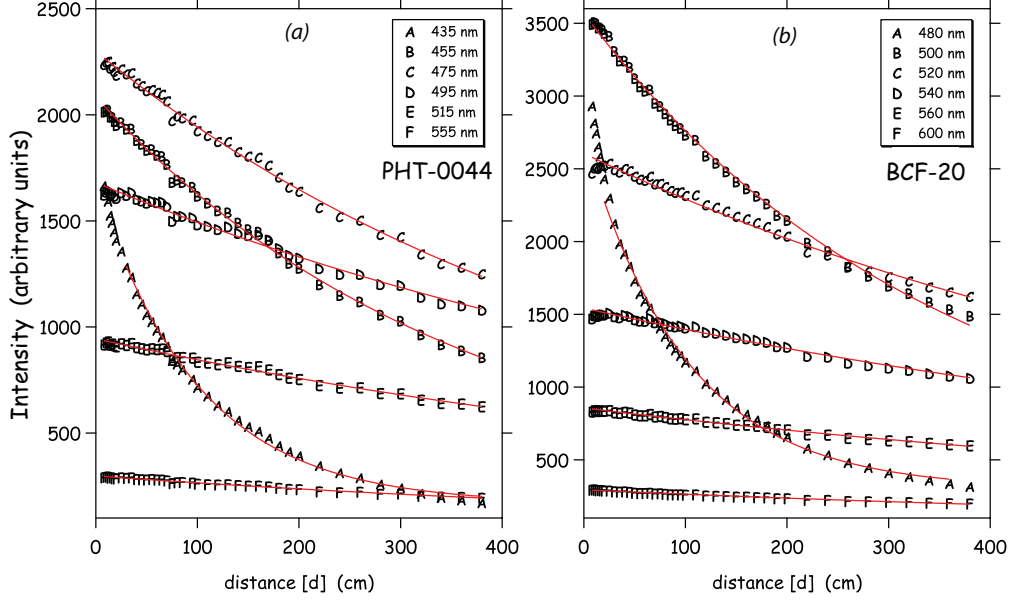


Fig. 7. Integrals of the Moyal fits to the spectral functions as a function of source distance for (a) the PHT-0044 and (b) the BCF-20 fibres. The points labeled *A* through *F* are the integrals for the wavelength ranges defined in Fig. 5. The curves are results of fits to a single exponential. More details are given in the text.

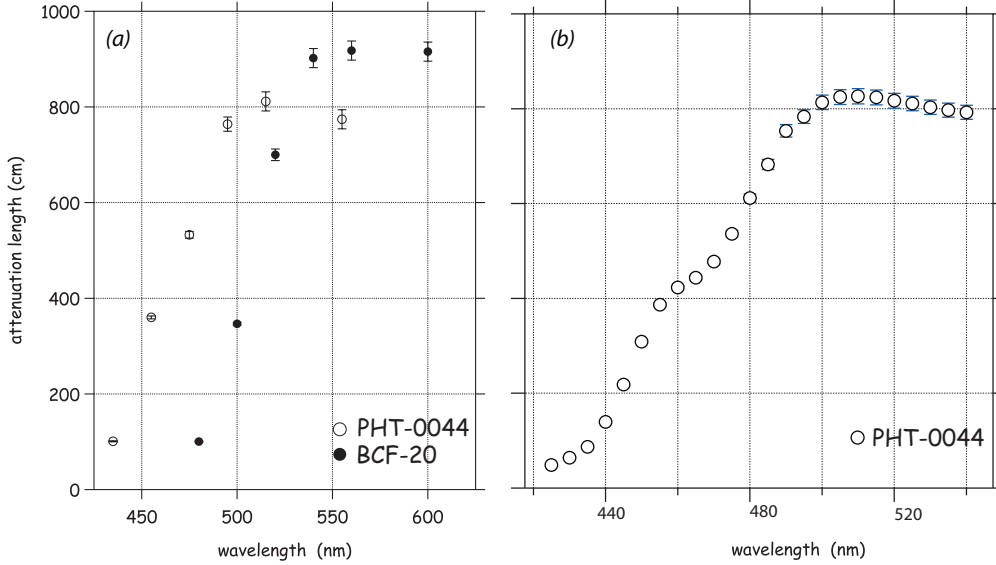


Fig. 8. (a) The attenuation length as a function of wavelength for the PHT-0044 and BCF-20 fibres. The attenuation length is the parameter λ as defined in Eq. 2 and is obtained by fitting the data shown in Fig. 7. (b) The attenuation length as a function of wavelength as extracted by plotting the value of the Moyal fit function as a function of distance at discrete wavelengths and fitting to an exponential. Note the structure in this dependence around 460 nm.

210 *4.3 Fibre spectral shape details*

211 The spectral shapes of the PHT-0044 and BCF-20 fibres differ significantly, as
 212 can be seen in Figs. 4 and 5. The striking difference between the PHT-0044

213 and BCF-20 fibres in terms of the loss of light from the source to 8 cm distance
 214 is illustrated in a graphical manner in Fig. 9. In that figure, the $d=0$ cm and
 215 8 cm spectra are shown as a function of wavelength, normalized at 490 nm
 216 and 590 nm for the PHT-0044 and BCF-20 fibres, respectively. The emission
 217 spectrum at the source ($d = 0$ cm) for the PHT-0044 fibre was assumed to
 218 follow the emission spectrum for BCF-12 as mentioned previously; that and
 219 the source spectrum for BCF-20 were provided by the manufacturer. This
 220 normalization was based on a combination of long attenuation length and
 221 sufficient intensity at each wavelength. With attenuation lengths of ~ 800 cm
 222 and ~ 900 cm at 490 nm and 590 nm, respectively, as extracted from Fig. 8,
 223 the effect of 8 cm in loss of strength is negligible. In addition, variations in the
 224 regions around these values resulted in stable ratios of areas under the spectral
 225 shapes, further emphasizing the lack of sensitivity to the exact normalization
 226 choice.

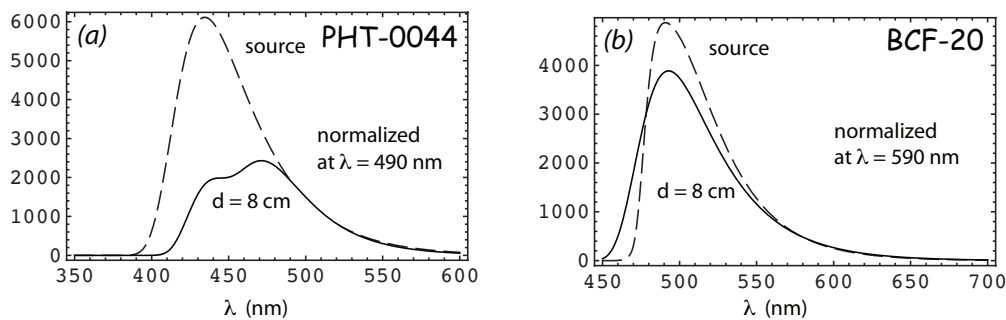


Fig. 9. The manufacturer's $d=0$ cm source (dashed line) and 8 cm spectra (solid line) are shown, as a function of wavelength for (a) the PHT-0044 and (b) BCF-20 fibres, respectively. Details are presented in the text.

227 The main features of Fig. 9 are: a) large loss of light from source to 8 cm for
 228 PHT-0044 as compared to the BCF-20 fibre and quantified in Section 4.4, and
 229 b) a curious discrepancy between the source and 8 cm curves for the BCF-20
 230 is apparent, where the latter extends to lower wavelengths. We have no firm
 231 explanation of this, however, a close inspection of the leading edge of the source
 232 shows a rather rapid (and unnatural in appearance) rise from its 470 nm base
 233 to its 490 nm peak. A possible explanation is that the manufacturer may have
 234 used a bandpass filter to block the blue wavelengths of a UV light source.

235 Our experimental setup used for the measurements, as presented in Section 3,
 236 did not allow measurements closer than 8 cm from the source. Therefore,
 237 in order to further investigate the double-peaked behavior of the PHT-0044
 238 spectra and to facilitate comparisons to the manufacturer's source spectra,
 239 we employed an alternate setup using the laser. In that, the laser light was
 240 transported via a clear optical fibre held by a clamp and a lab stand so as to be
 241 perpendicular to the tested PHT-0044 fibre, in a manner similar to the LED
 242 measurements. In this manner, a short sample (15 cm) of PHT-0044 fibre was
 243 tested by axially coupling it to a clear (BCF-90) 5 cm-long fibre using Q2-3067

244 optical grease¹⁰, with both fibres positioned in a channel of a plate so as to
 245 remain in contact and axially aligned. The clear fibre was threaded and epoxied
 246 through a SMA connector and facilitated proximity measurements of the PHT-
 247 0044 by bridging the gap from the spectro-photometer’s SMA connector to the
 248 CCD surface. In this manner, PHT-0044 spectra were collected at distances
 249 from 1 to 20 mm in 1 mm steps, from 20 to 60 mm in 5 mm steps and
 250 at 100 mm. The latter point provided an “anchor point” to the LED data,
 251 since the two measurements had different setups. Indeed, it was reassuring to
 252 observe that the LED- and laser-stimulated PHT-0044 spectra at 10 cm were
 253 consistent, as shown in Fig. 10.

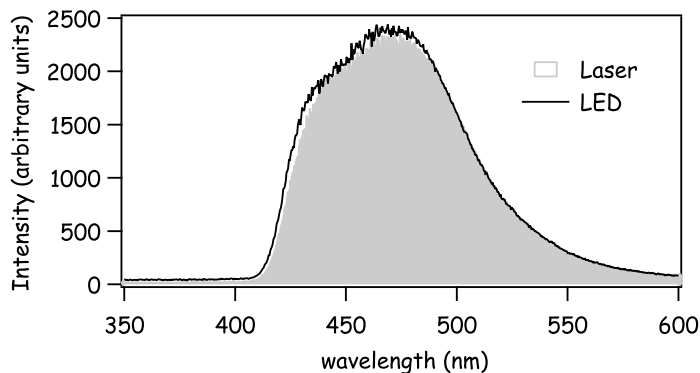


Fig. 10. A comparison of the spectra for PHT-0044 with two different excitation sources at a distance of 10 cm. The LED spectrum was taken with the 4-m PHT-0044 fibre in 2007 and the UV laser spectrum was taken using a short PHT-0044 sample in 2008. No normalization was applied in the display of these curves, although attention was paid at the measurement stage to approximately match the intensity of the laser to that of the LED, as measured in the spectro-photometer. The small differences could be attributed to the different wavelength ranges stimulated by the LED and laser, as shown in Fig. 1 and/or from the “extended” beam projection of the LED compared to that of the laser fibre tip.

254 Having assured the reliability of the laser measurements, the resultant spectra
 255 are shown in Fig. 11, normalized at 500 nm. Normalization at other wave-
 256 lengths was carried out, but the 500 nm normalization was the most consistent
 257 one, since the high-wavelength tails of all distance measurements overlapped
 258 perfectly, and no large discrepancies appeared at the two peaks. Of course,
 259 some deviation of the curves is expected on the low-wavelength side due to
 260 absorption, and this is exactly what is observed. Additional analysis cross
 261 checks, such as Moyal fits and spectral integrations, verified this behavior.
 262 Since the laser measurements aimed at a qualitative understanding of the
 263 double-peaked behavior of the PHT-0044 data and a cross-check of the LED
 264 data, further quantitative analysis was deemed beyond the scope of this paper.

265 The spectra at distances of a few mm’s from the excitation source should

¹⁰ Dow Corning Corporation, Midland, MI, USA (www.dowcorning.com)

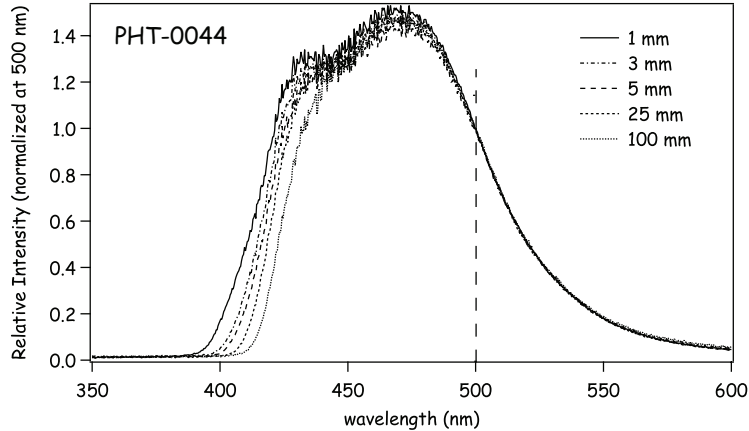


Fig. 11. Measurements from a short sample of PHT-0044 fibre using the UV laser. Spectra were collected at distances from 1 to 20 mm in 1 mm steps, from 20 to 60 mm in 5 mm steps and at 100 mm, but only five of them are shown for reasons of clarity. The spectra were normalized relative to each other at the wavelength value of 500 nm.

266 closely match the “source spectrum” provided by the SciFi manufacturers.
 267 For PHT-0044 (and BCF-12), however, the peak emission is listed by them
 268 at 435 nm with no evidence of secondary strength at 460-470 nm. Our mea-
 269 surements are in disagreement to those reference spectra: while some strength
 270 is evident at 435 nm, the peak emission is at 460-470 nm, instead. One ex-
 271 planation may lie in the attenuation length measurements, shown in Figs. 7
 272 and 8. The attenuation length at 460 nm is ~ 400 cm, compared to ~ 80 cm at
 273 435 nm. Thus, if the source spectrum has secondary emission strength around
 274 460-470 nm, the reduced attenuation of the latter compared to the former can
 275 result in the double-peak structure observed in our measurements. It is worth
 276 noting here that the blue emitting fibres in reference [3], the equivalent fibre
 277 types from Kuraray (SCSF-81 and SCSF-81M)¹¹, and several blue-emitting
 278 plastic scintillator data (BC-400, BC-404 and BC-408 from St. Gobain as well
 279 as EJ-200 from Eljen¹²) all show a “shoulder” in the source emission spectra
 280 in the region of 460-470 nm.

281 The significant difference in attenuation lengths at 435 nm and 460-470 nm
 282 can easily provide the explanation of the structure observed in Fig. 5. How-
 283 ever, the attenuation length for 435 nm cannot account for the weak strength
 284 observed at a few mm distance from the source location. Another mechanism
 285 must be responsible for the suppressed emission at the nominal peak wave-
 286 length of 435 nm. Taking into consideration that the reference spectra are
 287 generated within scintillation material thickness of 1 cm or more, it is possible
 288 that within the 1 mm diameter (maximum effective thickness) of the fibre
 289 the UV source does not fully excited the dyes, thus resulting in a reduced

¹¹ Kuraray America Inc., Houston, TX, USA (www.kuraray-am.com)

¹² Eljen Technology, Sweetwater, TX, USA (www.eljentechnology.com)

290 strength at the lower wavelengths. The 10 cm distance spectra for BCF-12 in
291 reference [8] appear very similar to those shown in Figs. 5 and 10 of this work.
292 The agreement between the reference spectra and our measurements for BCF-
293 20 further indicates that this effect is indeed confined to lower wavelengths.

294 A quick calculation from our work shows that the resolving power, $R = \lambda/\Delta\lambda$,
295 of our LED and laser is 28.6 and 375, respectively. Coupled to the aforemen-
296 tioned spectro-photometer resolution of 0.3 nm, these values result in a very
297 fine resolution in wavelength, that does not appear to be the case for the re-
298 sults in reference [9], which is perhaps why the second peak appears to be
299 washed out in their work and other published data.

300 4.4 *Scintillating fibre/photosensor matching*

301 The fibre spectra of intensity versus wavelength in Fig. 12a were convoluted
302 with the spectral response of a typical bi-alkali PMT (the XP2020¹³) and a
303 SiPM (the A35H SiPM¹⁴) in Fig. 12b, respectively, resulting in the curves
304 shown in Fig. 12c and Fig. 12d.

305 Specifically, the PHT-0044 and BCF-20 spectra were convoluted over wave-
306 length with the XP2020 QE and SiPM PDE, respectively, and were plotted as
307 a function of distance from the source. Double-exponential fits were employed
308 with two attenuation lengths (short and long). Note that when the PHT-044
309 spectrum is folded with the XP2020 QE, the fraction of the integrated source
310 intensity (see Fig. 9a) seen at 200 cm from the source is 24% while the cor-
311 responding fraction for the BCF-20 with the A35H is 61%. Since the QE and
312 PDE are relatively flat in the region of interest, these fractions reasonably de-
313 scribe the actual loss of light in the fibres. One can conclude that, whereas the
314 integrated intensity of the PHT-0044 fibre coupled to the XP2020 is superior
315 to that of the BCF-20 fibre, the results are indistinguishable when the fibres
316 are coupled to the SiPM, only if one considers the data in the $d = 8-380$ cm
317 region, and not from the source.

318 The wavelength-averaged QE of the XP2020 and PDE of the A35H SiPM were
319 computed using the emission spectra of PHT-044 and BCF-20. The integrals
320 of these spectra over wavelength were computed as a function of distance,
321 with and without convolution with the QE (or PDE), by dividing the integral
322 with convolution by the integral without convolution. The results are shown
323 in Fig. 13. For PHT-044, at 200 cm from the source, the average QE of the
324 XP2020 is 15% and that of the A35H is 14%. For BCF20, at 200 cm from the
325 source, the average QE of the XP2020 is 9% and that of the A35H is 14%.

¹³ PHOTONIS SAS, Brive, France (www.photonis.com).

¹⁴ A prototype SiPM from SensL with a $35\mu\text{m}$ pixel pitch.

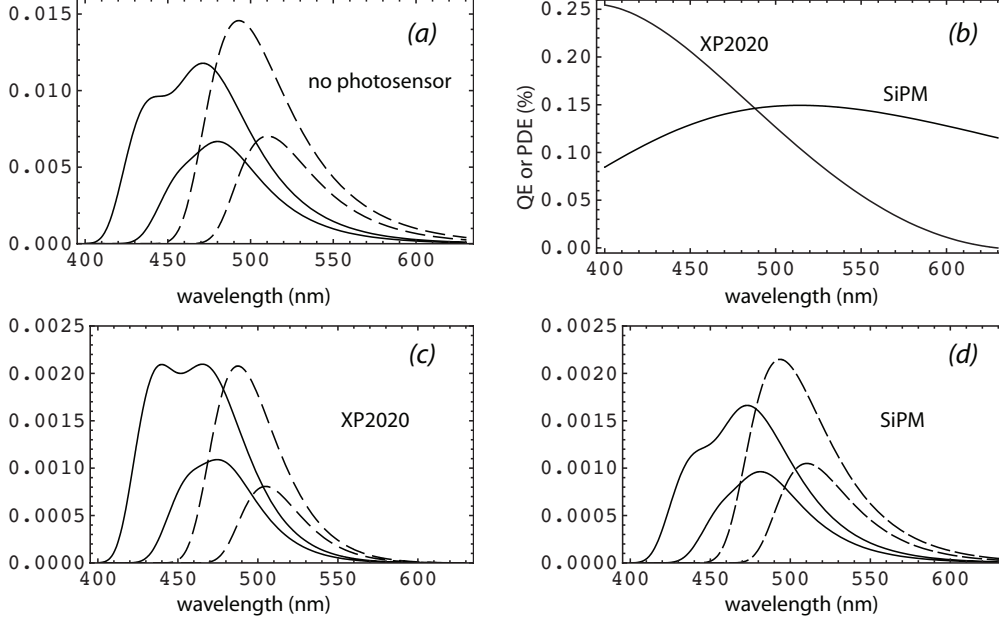


Fig. 12. (a) Emission spectrum for the PHT-0044 (solid lines) and BCF-20 fibres (dashed lines) at 8 cm and 390 cm. The 8 cm spectra for both the blue and green fibres were normalized to give unity for the respective total integrals. (b) The QE and PDE for the XP2020 and SiPM respectively. (c) The PHT-0044 and BCF-20 spectra now convoluted with the QE of the XP2020. Note that the areas under the curves for the 8 cm distance are set to 1.0 in plot (a), which results in areas under the PHT-0044 spectra of 0.164 and 0.068 while those under the BCF-20 curves are 0.110 and 0.040, both in plot (c). (d) Similar curves, but now convoluting with the PDE of the SiPM. The areas under the PHT-0044 curves are 0.136 and 0.067 while for the BCF-20 curves we have 0.145 and 0.065.

326 4.5 Attenuation length with and without photosensor

327 As can be seen in Fig. 7. the light output of a fibre is strongly dependent
 328 on λ and d , with shorter wavelengths that dominate at small distances be-
 329 ing replaced by longer wavelengths at larger distances. The bulk attenuation,
 330 however, is the result of the integrated light yield and, being the convolution
 331 of two different response regions, cannot be effectively represented by a single
 332 exponential function. Therefore, each fibre is thus characterized by a short
 333 and long attenuation length (see also Reference [11]). In order to extract these
 334 two components, a double exponential was used:

$$335 \quad I(d) = I_0 + \alpha_1 \cdot e^{-(d-d_0)/\lambda_1} + \alpha_2 \cdot e^{-(d-d_0)/\lambda_2} \quad (3)$$

336 Using this information, the attenuation length for PHT-0044 and BCF-20 was
 337 plotted with and without the photosensor coupling in Fig. 14. The fitted values
 338 from a double-exponential fit are shown in Table 1. The weighted attenuation
 339 length in that table is based on the relative amplitudes of the two exponentials.

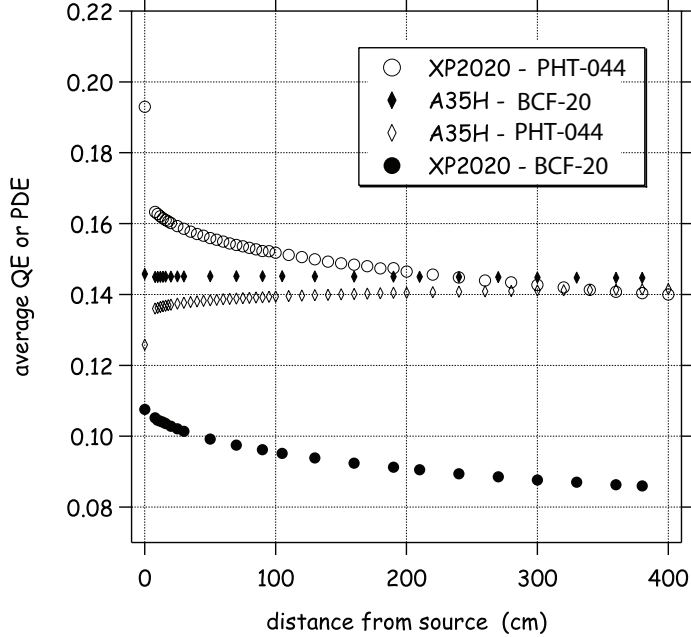


Fig. 13. The average QE of the XP2020 and the average PDE of the A35H, as a function of distance from source for PHT-044 and BCF-20 scintillating fibres, are shown. Details are given in the text.

340 The long bulk attenuation length of 414 cm for the PHT-0044 fibre combined
 341 with the XP2020 agrees well with the specification supplied by the manufactur-
 342 er, which was extracted using a ^{90}Sr electron source and a bi-alkali vacuum
 343 PMT. Those measurements were made between 64 cm and 200 cm and are
 344 dominated by the long component¹⁵. For the BCF-20 fibre, on the other hand,
 345 the manufacturer's specification was derived using bi-alkali PMT's and our re-
 346 sults cannot be compared directly to those. However, the smoothly varying
 347 and relatively flat QE response of a PMT over the emission spectrum of BCF-
 348 20 (approximately 460 nm to 560 nm; see Figs. 12b and 13) will not alter the
 349 weighted attenuation length of 408 cm, and St. Gobain quotes a value larger
 350 than 350 cm. In conclusion, our measurements using UV light sources and
 351 a spectral deconvolution agree very well with the manufacturer's ones using
 352 an electron source, once the range of distance measurements are taken into
 353 consideration.

354 4.6 Number of photoelectrons

355 In this section the number of photons at the end of each fibre will be calculated
 356 and used to determine the number of photoelectrons for two different readout

¹⁵ Information provided formerly by PolHiTech (www.polhitech.it)

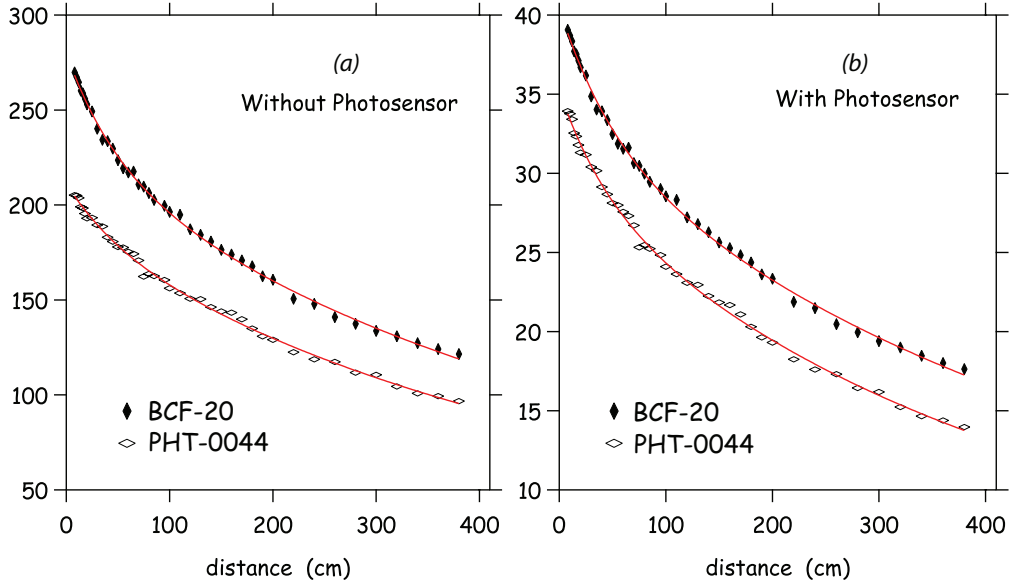


Fig. 14. Double-exponential fits to the PHT-0044 and BCF-20 data without and with the convolution of the photosensor. The photosensor in the case of PHT-0044 is the XP2020 and in the case of BCF20 is the SiPM. The results of the fits are shown in Table 1.

357 devices. These number will be compared to those extracted from our own
 358 beam tests [12].

359 SciFi's rely on total internal reflection for optical transmission. Manufacturers
 360 claim trapping efficiencies (capture ratio) around 3% and 5.5% for single- and
 361 double-clad fibres, respectively. These numbers reflect a simple calculation
 362 employing *meridional* optical rays. When *skew rays* are included, the trapping
 363 efficiency almost doubles [5]. The precise number for the trapping efficiency
 364 can be obtained only by Monte Carlo simulations and is slightly less than sum
 365 of the two terms, owing to the large path length of skew rays that results
 366 in losses. In the calculations below we assumed the manufacturer's (minimal)
 367 value.

368 When calculating the number of photons arriving at *one end* of either a BCF-
 369 12 (or equivalent type with peak emission at 435 nm) or BCF-20 fibre, one
 370 must start with the number of 8,000/MeV claimed by St. Gobain, which rep-
 371 represents the total number of photons created that travel to *both* ends of the
 372 fibre; then, the trapping efficiency *per side* and attenuation length must be
 373 applied to obtain the number of photons at the end of the fibre. Using this
 374 information, a minimum-ionizing, single-charged particle traversing a 1-mm-
 375 fibre will result in a few (2-6) photoelectrons at a few meters from the particle
 376 entry [3].

377 4.6.1 N_{pe} estimates from cosmic rays

378 A prototype BCAL module was built using PHT-0044 fibres and was tested
 379 using a photon beam and cosmic rays. The readout of the module was divided
 380 into 18 readout segments, comprised of six rows in depth and three columns
 381 vertically with respect to the beam. Acrylic light guides having a square profile
 382 and with a 45° mirrored surface channelled the light from the fibres to the
 383 PMTs that were placed perpendicularly to the fibre direction on both ends of
 384 the module [12].

385 The N_{pe} yield per segment side was extracted for minimum ionizing particles
 386 passing through the center of the BCAL module based on cosmic-ray mea-
 387 surements. The photoelectron yield is expected to be given by:

$$388 \quad N_{pe} = N_0 \cdot \delta E \cdot f_{survive} \cdot f_{PDE} \cdot f_{CR} \cdot f_{trans} \quad (4)$$

389 where:

- 390 (1) N_0 is the number of photons emitted by the scintillator per MeV of de-
 391 posited energy. We assume $N_0 = 8000$ photons/MeV, taken from the
 392 manufacturer's specifications;
- 393 (2) δE is the energy loss for a minimum ionizing particle passing through
 394 3.8 cm of the Pb/SciFi matrix that corresponded to the BCAL readout
 395 cell size during the beam test. This number was found to be 4.8 MeV,
 396 from simulations;
- 397 (3) $f_{survive}$ is the fraction of photons produced at the source that survive
 398 after 200 cm. From Section 4.4 we have $f_{survive} = 0.24$;
- 399 (4) f_{PDE} is the average photon detection efficiency for the XP2020 which is
 400 the average quantum efficiency (0.15 from Fig. 13) times 0.85 (average
 401 collection efficiency) or $f_{PDE} = 0.13$;
- 402 (5) f_{CR} is the capture ratio for double clad fibre. The manufacturer quotes
 403 a minimum $f_{CR} = 0.054$;
- 404 (6) f_{trans} is the transmission through the light guide used for BCAL Mod-
 405 ule 1. The 45° mirrored surface was measured to have a reflectivity of
 406 $\sim 75\%$ but the overall transmission, which also includes transmission
 407 through all the interfaces and coupling to the PMT was not measured.
 408 From simulations, an overall efficiency between 0.4 and 0.5 is expected.

409 Under the above assumptions, a range for $N_{pe} = 25 - 30$ is extracted, in good
 410 agreement to the measured $N_{pe} = 25.5 \pm 0.7$.

411 4.6.2 N_{pe} estimates for a 1 GeV photon

412 An estimated $N_{pe} = 770$ extrapolating to a 1 GeV photon was extracted from
413 the tests of the prototype module [12]. Following the same procedure as above,
414 Eq. 4 was used with $\delta E = f_{sample} \cdot 1000$ MeV and a sampling fraction of 12.5%
415 as estimated by the simulations. This resulted in a yield estimate of $N_{pe} \sim 700$,
416 in agreement with the measurement.

417 4.6.3 Estimating N_{pe} for green SciFi with SiPM

418 The weighted attenuation lengths for PHT-0044 and BCF-20 coupled to the
419 XP2020 and SiPM photosensors, tabulated in Table 1, show that neither com-
420 bination exhibits a clear superiority in terms of attenuation length. However,
421 with either SciFi generating 8,000 photons/MeV at the source, our results
422 indicate that the BCF-20 plus SiPM combination will deliver a factor of 2.5
423 more photons at 200 cm from the ionization source location than a PHT-0044
424 plus PMT combination. This is solely the result of the failure to populate the
425 435 nm peak in PHT-0044, as discussed in Section 4.3.

426 5 Summary and Conclusions

427 The relevant quantities in matching SciFi's to photosensors are the emission
428 spectra of the former and the spectral response of the latter because this
429 combination affects the number of photoelectrons generated independent from
430 attenuation length. Changes in the spectral emission of the fibre with length
431 affects the number of photoelectrons detected and introduces a non-linearity
432 in the energy response of the detector system. The combination of SiPM's
433 and fast green emitting SciFi's, such as BCF-20, in applications where the
434 technology of the latter is relevant, is an optimal one due to the flat PDE
435 response of the SiPM in the emission wavelength spectrum of the former and
436 the stability of the peak emission wavelength of the SciFi, as seen in Fig. 12.
437 Such combinations have already been reported in the literature [13].

438 Fast blue SciFi's are by far the most widely used fibres, in combination with
439 bi-alkali type of vacuum PMTs. Most such fibres with peak emission at nomi-
440 nal 435 nm – examples of which are PHT-0044 (now not available anymore),
441 BCF-12 and SCSF-81 – share very similar attenuation lengths and spectral
442 functions. However, our testing of several different samples produced consis-
443 tent emission spectra that are quite different than the manufacturers speci-
444 fications. In this paper we have shown only the results for PHT-0044 due to
445 the large detailed amount of experimentation that we have done with that
446 particular fibre. The peak emission is not at 435 nm, which appears only as

447 a secondary bump, but at approximately 470 nm, instead. One possible ex-
448 planation is that the thickness of the fibre presented to the exciting UV light
449 (maximum 1 mm) is not adequate to absorb the UV light and to allow its full
450 conversion to the emission spectrum representative of the material in sufficient
451 thickness. As such, the emission spectra in this paper near the illumination
452 center, shown in Fig. 11, are the effective spectra for such types of fibres.

453 This observation leads to question the effective photon yield listed by most
454 manufacturers of approximately 8,000 photons/MeV of deposited energy by
455 minimum ionizing particles (MIP). If such yield is the integral of the full emis-
456 sion spectrum, as listed in the product literature, then a significant fraction,
457 approaching 50%, is not available for excitation by UV light, as shown in
458 Fig. 9. Experimental results are consistent with such reduced photon yields.
459 BCAL data with cosmic rays and photon beams verify that the nominal pho-
460 ton yield of 8,000/MeV has to be reduced by a significant fraction, over and
461 above that justified by attenuation length and spectral distortion with dis-
462 tance, to account for the measured yields. The same treatment was applied
463 to the KLOE results of 700 photoelectrons for 1 GeV incident photon en-
464 ergy [10] taking into consideration the single-clad fibres used and the very
465 efficient light guide-Winston Cone collectors used. We then reproduced the
466 number of photoelectrons as measured by KLOE using Eq. 4 and the relevant
467 factors described in Section 4.6.1.

468 The conclusion derived here is that that our work explains the physics cause
469 for the commonly known fact that the measured number of photoelectrons
470 from SciFis do not reflect the theoretical number for scintillating material of
471 8,000/MeV. The actual number is closer to around 4,000 photons/MeV at the
472 scintillation location for 1 mm diameter blue emitting fibre.

473 Using the methodology described in this paper, it is concluded that the con-
474 version of UV light in 1 mm of BCF-20 material is much more efficient than
475 for blue fibres. The overlap of the reference and measured spectra in Fig. 9 is
476 significant, indicating a small loss of photon yield due to conversion to the final
477 emission spectrum. If this also represents the case of charged particle tracks in
478 BCF-20 fibres, as the results for PHT-0044 indicate, then one expects a fac-
479 tor of approximately 2.5 times the photoelectron yield of the BCF-20/SiPM
480 combination than obtained with the PHT-0044/PMT combinations.

481 It would be advisable for the manufacturers of scintillating fibres to show
482 actual spectra obtained in such thin materials, rather than reference emission
483 spectra than can only be realized in thicknesses beyond the realm of fibre
484 use and availability and to quote the effective number of photons per MeV of
485 energy deposit (MIP) produced in fibres.

486 Finally, the attenuation lengths of both PHT-0044 and BCF-20 are in good

487 agreement with specifications if the measurements duplicate the manufacturers
488 methodology. As such, both blue and green SciFi's exhibit comparable bulk
489 attenuation lengths with or without the influence of the two corresponding
490 types of photosensors used in our work.

491 **6 Acknowledgments**

492 This work was supported by NSERC grant SAPJ-326516 and DOE grant DE-
493 FG02-0SER41374 as well as Jefferson Science Associates, LLC. under U.S.
494 DOE Contract No. DE-AC05-06OR23177. Finally, many thanks must be given
495 to Alex Dzierba who contributed immensely to the analysis and writing of this
496 paper.

	Without Photosensor		With Photosensor	
Component	PHT-0044	BCF-20	PHT-0044	BCF-20
short (cm)	50 ± 14	48 ± 8	43 ± 8	50 ± 9
long (cm)	478 ± 21	481 ± 21	414 ± 14	491 ± 21
weighted (cm)	428 ± 23	400 ± 23	353 ± 18	408 ± 25

Table 1

Short and long attenuation length components for the PHT-0044 and BCF-20 fibres, as extracted from a double-exponential fit. The weighted attenuation length is based on the relative amplitudes of the two exponentials. The photosensor in the case of PHT-0044 is the XP2020 and in the case of BCF-20 is the SiPM.

497 **Figure Captions**

498 **Fig. 1.** Emission and absorption spectra from the secondary dye of (a) BCF-12
499 and (b) BCF-20 fibres. Also shown are the stimulated wavelength ranges from
500 the 373 nm LED and 375 nm laser used in our measurements, as discussed
501 below. All curves have been arbitrarily normalized to facilitate the comparison
502 of their spectral shapes. (colour online)

503 **Fig. 2.** Comparison of the emission spectra of the LED and the laser as
504 measured directly, using the spectro-photometer, and plotted on a logarithmic
505 scale. Details are provided in the text. (colour online)

506 **Fig. 3.** Schematic drawing of the experiment. The test fibre is shown as the
507 bold horizontal line: on the right it is clamped to a lab stand (C), in the
508 middle it threads through the legs of the LED support stand via barrels (B)
509 having 1 mm inner diameter holes and external threads that mount on the
510 support frame and on the left it is connected to the slave channel (S) of the
511 SD2000 spectro-photometer by an SMA connector. The SD2000 connects to
512 the ADC via a flat-ribbon bus and the ADC, in turn, connects to a PC via
513 a USB cable. The vertical arrow pointing downwards from the LED housing
514 indicates the direction of the incident light through its port (P) onto the test
515 fibre. The horizontal displacement of the light direction to the entrance of
516 the SD2000 master channel is our distance parameter, z . This figure is not to
517 scale: for example, the LED's port is a lot closer to the fibre than implied in
518 this schematic.

519 **Fig. 4.** (a) The emission spectrum for the BCF-20 fibre (grey band) is shown
520 with the source located at 8 cm from the spectro-photometer and the results
521 of a fit (dashed line) to a Moyal function plus a flat background; and (b) The
522 emission spectrum (grey band) for the PHT-0044 fibre with the source located
523 at 8 cm from the spectro-photometer with the results of a fit (dashed line) to
524 a sum of two Moyal functions plus a flat background.

525 **Fig. 5.** The results of fits to Moyal functions for spectral measurements at
526 source distances ranging from 8 to 380 cm for (a) PHT-044 and (b) BCF-
527 20 fibres. The wavelength ranges labeled A through F in the plots will be
528 referenced later in this paper. (colour online)

529 **Fig. 6.** Dependence of the Moyal fit parameters (a) μ and (b) σ as a function
530 of source distance for the PHT-0044 and BCF-20 fibres.

531 **Fig. 7.** Integrals of the Moyal fits to the spectral functions as a function of
532 source distance for (a) the PHT-044 and (b) the BCF-20 fibres. The points
533 labeled A through F are the integrals for the wavelength ranges defined in
534 Fig. 5. The curves are results of fits to a single exponential. More details are

535 given in the text.

536 **Fig. 8.** (a) The attenuation length as a function of wavelength for the PHT-
537 044 and BCF-20 fibres. The attenuation length is the parameter λ as defined in
538 Eq. 2 and is obtained by fitting the data shown in Fig. 7. (b) The attenuation
539 length as a function of wavelength as extracted by plotting the value of the
540 Moyal fit function as a function of distance at discrete wavelengths and fitting
541 to an exponential. Note the structure in this dependence around 460 nm.

542 **Fig. 9.** The manufacturer's $d=0$ cm source (dashed line) and 8 cm spectra
543 (solid line) are shown, as a function of wavelength for (a) the PHT-0044 and
544 (b) BCF-20 fibres, respectively. Details are presented in the text.

545 **Fig. 10.** A comparison of the spectra for PHT-0044 with two different exci-
546 tation sources at a distance of 10 cm. The LED spectrum was taken with the
547 4-m PHT-0044 fibre in 2007 and the UV laser spectrum was taken using a
548 short PHT-0044 sample in 2008. No normalization was applied in the display
549 of these curves, although attention was paid at the measurement stage to ap-
550 proximately match the intensity of the laser to that of the LED, as measured
551 in the spectro-photometer. The small differences could be attributed to the
552 different wavelength ranges stimulated by the LED and laser, as shown in
553 Fig. 1 and/or from the "extended" beam projection of the LED compared to
554 that of the laser fibre tip.

555 **Fig. 11.** Measurements from a short sample of PHT-0044 fibre using the UV
556 laser. Spectra were collected at distances from 1 to 20 mm in 1 mm steps, from
557 20 to 60 mm in 5 mm steps and at 100 mm, but only five of them are shown
558 for reasons of clarity. The spectra were normalized relative to each other at
559 the wavelength value of 500 nm.

560 **Fig. 12.** (a) Emission spectrum for the PHT-0044 (solid lines) and BCF-20
561 fibres (dashed lines) at 8 cm and 390 cm. The 8 cm spectra for both the blue
562 and green fibres were normalized to give unity for the respective total integrals.
563 (b) The QE and PDE for the XP2020 and SiPM respectively. (c) The PHT-
564 0044 and BCF-20 spectra now convoluted with the QE of the XP2020. Note
565 that the areas under the curves for the 8 cm distance are set to 1.0 in plot
566 (a), which results in areas under the PHT-0044 spectra of 0.164 and 0.068
567 while those under the BCF-20 curves are 0.110 and 0.040, both in plot (c).
568 (d) Similar curves, but now convoluting with the PDE of the SiPM. The areas
569 under the PHT-0044 curves are 0.136 and 0.067 while for the BCF-20 curves
570 we have 0.145 and 0.065.

571 **Fig. 13.** The average QE of the XP2020 and the average PDE of the A35H,
572 as a function of distance from source for PHT-044 and BCF-20 scintillating
573 fibres, are shown. Details are given in the text.

574 **Fig. 14.** Double-exponential fits to the PHT-0044 and BCF-20 data without
575 and with the convolution of the photosensor. The photosensor in the case of
576 PHT-0044 is the XP2020 and in the case of BCF20 is the SiPM. The results
577 of the fits are shown in Table 1.

578 **References**

- 579 [1] GlueX/Hall D Collaboration, The Science of Quark Confinement and Gluonic
580 Excitations, GlueX/Hall D Design Report, **Ver.4** (2002).
581 (<http://www.phys.cmu.edu/halld>).
- 582 [2] A.R. Dzierba, C.A. Meyer and E.S. Swanson, *American Scientist*, **88**, 406
583 (2000).
- 584 [3] A.J. Davis *et al.*, *Nucl. Instr. and Meth. A* 276 (1989) 347.
- 585 [4] Yu.G. Kudenko, L.S. Littenberg, V.A. Mayatski, O.V. Mineev and N.V.
586 Yershov, *Nucl. Instr. and Meth. A* 469 (2001) 340.
- 587 [5] C.P. Achenbach, arXiv:nucl-ex/0404008 v1, (2004).
- 588 [6] R.C. Ruchti: *Ann. Rev. Nucl. Part. Sci.* 46 (1996) 281.
- 589 [7] J. E. Moyal, *Phil. Mag.* 46 (1955) 263.
- 590 [8] G. Drexlin, V. Eberhard, D. Hunkel and B. Zeitnitz, *Nucl. Instr. and Meth. A*
591 360 (1995) 245.
- 592 [9] L. Archambault *et al.*, *Med. Phys.* 32 (7) (2005) 2271.
- 593 [10] A. Antonelli *et al.*, *Nucl. Instr. and Meth. A* 370 (1996) 367.
- 594 [11] K.V. Alexandrov *et al.*, *Nucl. Instr. and Meth. A* 459 (2001) 123.
- 595 [12] B.D. Leverington *et al.*, GlueX-doc-1071-v1 (<http://portal.gluex.org/>,
596 Documents, Public), Technical Report, GlueX Collaboration, 2007; submitted
597 to *Nucl. Instr. and Meth. A* (2008).
- 598 [13] H. Gast *et al.*, arXiv:0711.4694v1 [physics.ins-det] 29 Nov 2007.